

RESEARCH LETTER

10.1002/2014GL061281

Key Points:

- Haiyan (2013) was one of the most intense tropical cyclones ever observed
- Two key factors for Haiyan's extra-ordinary intensification were discovered
- Warm subsurface water and fast typhoon travelling speed

Correspondence to:

I.-I. Lin,
iilin@as.ntu.edu.tw

Citation:

Lin, I.-I., I.-F. Pun, and C.-C. Lien (2014), "Category-6" supertyphoon Haiyan in global warming hiatus: Contribution from subsurface ocean warming, *Geophys. Res. Lett.*, 41, doi:10.1002/2014GL061281.

Received 23 JUL 2014

Accepted 20 SEP 2014

Accepted article online 4 OCT 2014

"Category-6" supertyphoon Haiyan in global warming hiatus: Contribution from subsurface ocean warming

I.-I. Lin¹, Iam-Fei Pun¹, and Chun-Chi Lien¹¹Department of Atmospheric Sciences, National Taiwan University, Taipei, Taiwan

Abstract With the extra-ordinary intensity of 170 kts, supertyphoon Haiyan devastated the Philippines in November 2013. This intensity is among the highest ever observed for tropical cyclones (TCs) globally, 35 kts well above the threshold (135kts) of the existing highest category of 5. Though there is speculation to associate global warming with such intensity, existing research indicate that we have been in a warming *hiatus* period, with the *hiatus* attributed to the La Niña-like multi-decadal phenomenon. It is thus intriguing to understand why Haiyan can occur during *hiatus*. It is suggested that as the western Pacific manifestation of the La Niña-like phenomenon is to pile up warm subsurface water to the west, the western North Pacific experienced evident subsurface warming and created a very favorable ocean pre-condition for Haiyan. Together with its fast traveling speed, the air-sea flux supply was 158% as compared to normal for intensification.

1. Introduction

Super-typhoon Haiyan, at its peak intensity of 170 kts (in 1 min maximum sustained surface wind speed from the US Joint Typhoon Warning Center), made landfall to the Philippines on 8 November 2013. The strong storm surge [Mori *et al.*, 2014], astonishingly intense wind, and associated rain brought catastrophic destruction to the country [Lander *et al.*, 2014]. In fact, Haiyan's intensity can be considered as "a league" higher than the majority of existing category 5 (in Saffir-Simpson scale, Table 1a) TCs worldwide (further details see section 4 and supplementary) [Knapp *et al.*, 2010; Lander *et al.*, 2014]. However, we have been in the global warming hiatus period, and the warming has paused for more than a decade [Kosaka and Xie, 2013; England *et al.*, 2014]. It is thus of much interest to understand why Haiyan can reach such high intensity during the hiatus and why they can coexist.

The recent global warming hiatus is attributed to a La Niña-like decadal cooling phenomenon over the eastern tropical Pacific Ocean [Kosaka and Xie, 2013]. Recent work by Kosaka and Xie [2013] demonstrated that this ongoing cooling can cool the planet and offset the global warming. However, the manifestation of this phenomenon is cooling over the east but *warming* over the western tropical Pacific. The associated strengthening of the easterly wind piles up warm ocean surface water to the west [Kosaka and Xie, 2013; Wang *et al.*, 2013; England *et al.*, 2014] (Figure 1a). As a result, western Pacific is accumulated with thicker layer of warm water and high sea level [Cazenave and Remy, 2011; Qiu and Chen, 2012], especially at the east of the Philippines where Haiyan intensified (Figures 1b and 1c).

All of the above set up an optimal stage awaiting Haiyan. The high sea level rise in itself could increase its damage on land because of possible contribution to stronger storm surge [Forbes *et al.*, 2010; Lin *et al.*, 2013b] (Figures 1b and 1c). The warm water accumulation has caused subsurface ocean to warm up (as characterized by increased ocean heat content and subsurface depth-average temperature) to reach the highest value in 2 decades (Figure 2a).

We also observed that the strong easterly wind [Wang *et al.*, 2013; Kosaka, 2014] pushed Haiyan to travel very fast ($\sim 9 \text{ m s}^{-1}$) (Figures 1, S2, and S3). Both subsurface ocean warming (characterized by high subsurface temperature/heat content) and fast traveling speed have strong implications on ocean's energy supply for Haiyan's intensification [Shay *et al.*, 2000; Lin *et al.*, 2009], as discussed below.

2. Preexisting Warm Subsurface Condition and Haiyan's Fast Traveling Speed

TC's intensification requires favorable storm structure, atmospheric (e.g., weak vertical wind shear) and ocean conditions [Gray, 1979; Emanuel, 1988, 1999; Frank and Ritchie, 2001; Emanuel *et al.*, 2004;

Table 1a. Saffir-Simpson Tropical Cyclone Scale From Category 1 to 5, and the Proposed Empirical Category "6"^a

TC Category		Wind speed (kts)
1		64-82
2	19	83-95
3	13	96-113
4	18	114-135
5	22	>135
'6' ? (empirical)	20	>155 [Haiyan: 170 kts]

^aAs the gap between each consecutive category is from 13 to 22 kts (indicated between categories), 155 kts is used as a possible minimum for category "6" (i.e., 20 kts above the current category 5 threshold).

Lin et al., 2005; Cione et al., 2013]. Ocean is a critical necessary condition because it is the source of energy supply. Not only warm sea surface temperature (SST), warm subsurface ocean temperature (often characterized by T100, depth-averaged temperature of upper 100 m of ocean [Price, 2009]) and high heat content (or called TCHP, Tropical Cyclone Heat Potential) are also important for intensification [Leipper and Volgenau, 1972; Shay et al., 2000; Emanuel et al., 2004; Lin et al., 2005, 2008, 2013a; Yablonski and Ginis, 2008; Goni et al., 2009; Pun et al., 2007, 2013, 2014; Seo and Xie, 2013]. Under normal condition, the intense TC wind inevitably mixes the colder subsurface water to surface [Price, 1981; Price et al., 1994; Bender and Ginis, 2000; Cione and Uhlhorn, 2003]. Consequentially, SST and hence energy supply (i.e., enthalpy (sensible + latent) heat fluxes) from ocean to TC reduces [Emanuel, 1999; Bender and Ginis, 2000; Emanuel et al., 2004; Lin et al., 2013a]. This is known as the cooling effect [Price, 1981; Price et al., 1994; Bender and Ginis, 2000]. However, if pre-TC subsurface ocean temperature is warm and T100 (or TCHP) is high, the cooling effect can be effectively suppressed, and more energy can be supplied during TC's intensification, a condition important for intense TCs (e.g., supertyphoons) [Shay et al., 2000; Lin et al., 2005, 2008, 2013a; Yablonski and Ginis, 2008; Goni et al., 2009; Pun et al., 2013; Seo and Xie, 2013].

Before Haiyan's occurrence, Pun et al. [2013] already alerted the possibility of increasing chance for supertyphoons in this region, because T100 and TCHP were much higher than normal (Figure 2a). As observed by the Argo in situ floats, thick layer of warm water (red profiles in Figure 2b) preexisted before Haiyan's arrival, an "add on" to an existing relatively warm condition (black profiles).

Haiyan's fast traveling speed further contributed to suppress the cooling effect because cooling effect is smaller when TCs are fast traveling (less time for ocean to respond to the TC wind) [Price, 1981; Price et al., 1994; Lin et al., 2009]. Based on 42 years' (1970–2011) of typhoon records, we calculated the traveling speed for all 1232 typhoons. In Figure 1e, it can be found that 5 m s⁻¹ is the most commonly observed TC traveling speed over this region. The observed 9 m s⁻¹ for Haiyan is a very fast speed with only about 1–3% of occurrence probability in the past 4 decades.

Table 1b. Exemplary Landfall Surface Wind Speed (V_{max} , Based on 1 min Maximum Sustained Surface Wind Speed) and Wind Speed Cube (V_{max}^3), for Different TC Categories^a

Exemplary landfall wind speed (kts)		V_{max}^3 Cube of landfall wind speed (kts ³)
65 (category 1)		274,625
85 (category 2)	×2.2	614,125
100 (category 3)	×1.6	1,000,000
115 (category 4)	×1.5	1,520,875
140 (category 5)	×1.8	2,744,000
170 (category '6?') [Haiyan (2013)]	×1.8	4,913,000

^aThe numbers between the consecutive categories indicate the proportional increase in landfall V_{max}^3 . It can be seen in column 2 that the landfall V_{max}^3 of Haiyan is 180% as compared to a regular category 5 TC of 140 kts. It thus can be risky if the public equate Haiyan as a regular category 5 at landfall. At the moment, because there is no category "6", Haiyan is categorized as category 5 at landfall.

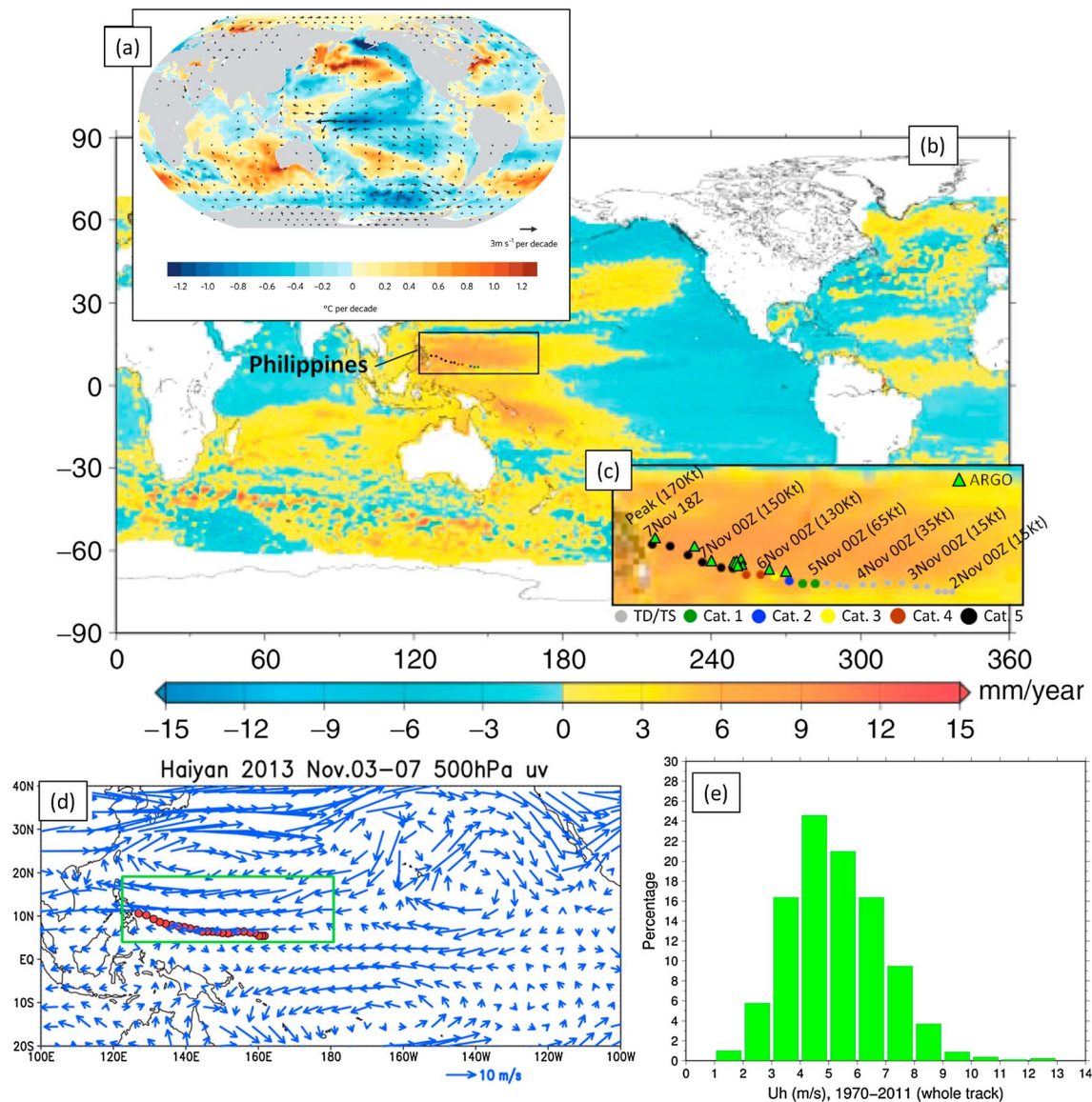


Figure 1. (a) Sea surface temperature (SST) and surface wind velocity decadal trends based on monthly anomalies of NOAA OISST and ECMWF interim data sets from 2001 to 2013 (after *Kosaka* [2014]). Easterly trade wind (westward vectors) strengthens in the Pacific, leading to divergence around the equator (blue shading) and accumulation of warm water (yellow shading) in the western North Pacific where Haiyan intensified (after *Kosaka* [2014]). (b) Haiyan's intensification region (box) on the global sea level trend map. The map is from satellite altimetry observations over 1993–2009 with respect to the global mean rise (i.e., a uniform mean trend of 3.3 mm/year is removed) (after *Cazenave and Remy* [2011]). The sea level rise over this region is the highest on earth, four times of global average. (c) Zoom of the box in Figure 1b, with Haiyan's track and intensity overlaid. Locations of the pre-Haiyan Argo profiles (red profiles in Figure 2b) are shown in green triangles. (d) Prevailing environmental wind condition during Haiyan's intensification period (3–7 November 2013) at 500 hPa. The track and the intensification location (see box) of Haiyan are also depicted. Data source: ECMWF operational atmospheric data. (e) Statistics of the TC traveling speed distribution over the study domain, based on 42 years' (1970–2011) of typhoon records from the JTWC data base (1232 cases).

3. TC-Induced Ocean Cooling Effect and Air-sea Enthalpy Fluxes

To quantify the control of warm subsurface ocean water layer and fast traveling speed on Haiyan, we conducted numerical simulations under four scenarios using the three-dimensional Price-Weller-Pinkel ocean mixed layer model (3DPWP) [*Price et al.*, 1994] (Supplementary Online Material (SOM)). Scenario 1 (4) is the observed (normal) scenario, i.e., with (without) the two favorable factors. Scenario 2 (3) simulates the situation with only the fast traveling speed (warm ocean) favorable factor. As in Figure S4, due to the two favorable factors, the cooling effect was very minimal ($\sim 0.5^\circ\text{C}$) throughout Haiyan's intensification (red curve). Without them (brown curve), the cooling effect is evidently stronger ($\sim 2.3^\circ\text{C}$).

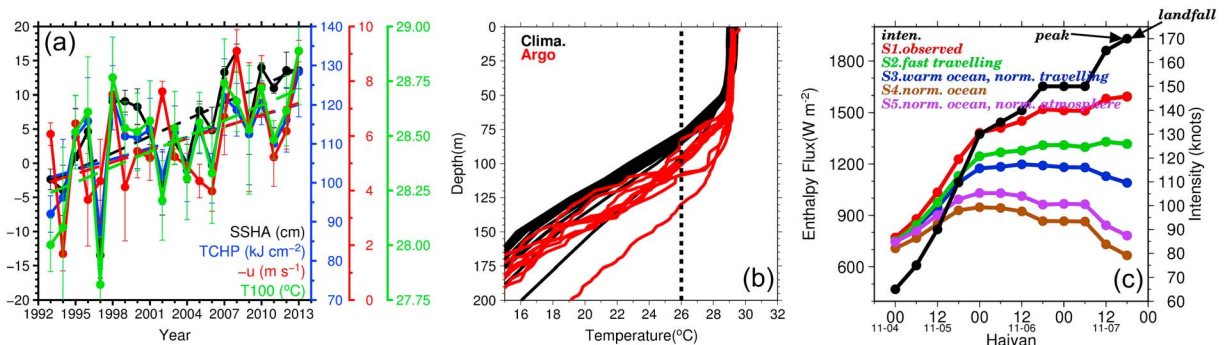


Figure 2. (a) More than 2 decades (1993–2013) of observations show that over the western Pacific tropical cyclone (TC) Main Development Region (MDR) at the east of the Philippines (box in Figure 1b), Tropical Cyclone Heat Potential (TCHP) (typhoon season average), T100 (typhoon season average), sea surface height anomaly (typhoon season average), and easterly wind (averaged between 850 and 500 hPa, 3–7 November) all have increased significantly and peaked in 2013. (b) Ocean’s preexisting thermal condition for Haiyan, as observed by Argo floats (red profiles, acquired within 5 days prior to Haiyan, locations see Figure 1c). The black profiles are for comparison, showing the normal, climatological ocean condition. (c) Series of numerical experiments showing ocean’s energy supply (i.e., enthalpy heat fluxes) for Haiyan’s intensification under five scenarios: 1. the observed scenario (red curve, with preexisting warm water accumulation and fast TC traveling speed of 8.9 m s^{-1}); 2. normal ocean but still with fast traveling speed of 8.9 m s^{-1} (green curve); 3. with warm water accumulation but normal traveling speed of 5 m s^{-1} (blue curve); 4. normal ocean and normal traveling speed (brown curve); 5. normal ocean, normal traveling speed, and normal atmosphere (purple curve). Haiyan’s intensity is also plotted (black curve, right axis).

After quantifying the cooling effects, sensible and latent heat fluxes (SHF and LHF) are calculated, based on the bulk aerodynamic formula under TC–ocean coupling condition [Cione *et al.*, 2013; Lin *et al.*, 2013a] as follows:

$$\text{SHF } Q_S = C_H W (T_s - T_a) \rho_a C_{pa}$$

$$\text{LHF } Q_L = C_E W (q_s - q_a) \rho_a L_{va}$$

where C_H and C_E are the sensible and latent heat exchange coefficients, W is ocean surface wind speed, T_s and T_a are during-TC SST and near surface air temperature, q_s and q_a are surface and air specific humidity, and ρ_a , C_{pa} , and L_{va} are air density, heat capacity of the air, and latent heat of vaporization. For Scenarios 1–4, the same observed atmospheric T_a and q_a data from November 2013 was used; therefore, the variability in flux is only due to change in ocean cooling effect.

To make additional assessment if atmospheric condition also changes, we added the 5th scenario in flux calculation. Scenario 5 has the same ocean cooling as scenario 4, but with additional change in the atmospheric condition. The input was based on the climatological T_a and q_a (for the month of November, based on the 1993–2012 average). Therefore, scenario 5 indicates the flux supply under “normal ocean + normal atmosphere” condition.

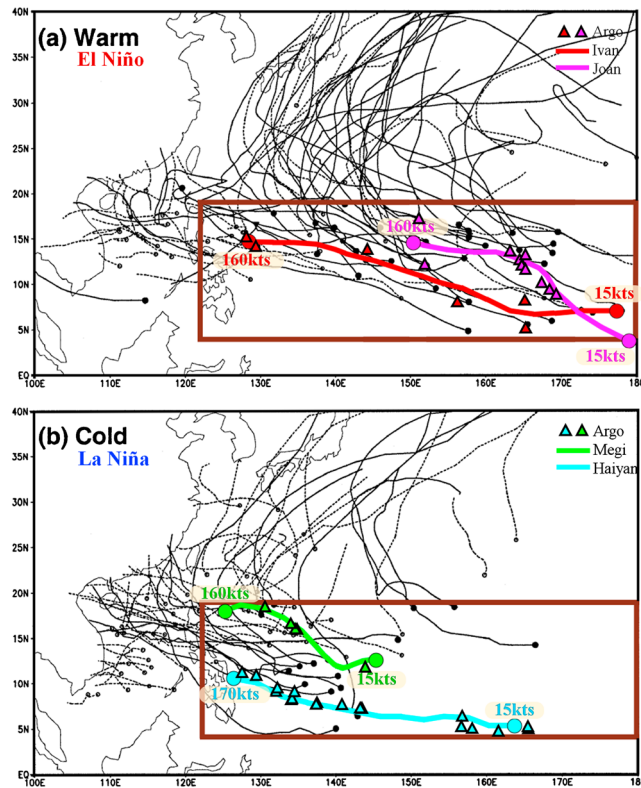
From the flux results, it can be seen that Scenario 1 has 58% (44%) excessive flux supply wrt normal (Scenarios 4 (5), Figure 2c and Table S1). Further, it would be difficult for Haiyan to intensify to the observed 170 kts (black curve) under Scenarios 4 and 5, since the energy supply starts to decline around 6 November onward (brown and purple curves in Figure 2c).

This also explains why under normal condition over this region, it is possible to support intensification of regular category 5 typhoons (mostly 140 kts, see black curve around 6 November 2014, in Figure 2c) [Lin *et al.*, 2008, 2009; Goni *et al.*, 2009; Knapp *et al.*, 2010]. However, to support up to the 170 kts intensity like Haiyan (i.e., continual intensification beyond 6 November, black curve in Figure 2c), additional energy supply is needed. The fast traveling speed and accumulation of warm water due to the La Niña-like phenomenon provided the opportunity for this additional supply.

4. Discussion and Conclusion

Besides the energy supply analyses, atmospheric vertical wind shear should be examined [Gray, 1979; Emanuel, 1999; Frank and Ritchie, 2001; Emanuel *et al.*, 2004]. As discussed in SOM, the shear condition was not optimal. Several unfavorable high shear periods were observed but did not appear to hinder Haiyan’s intensification (Figure S8).

From above, it can be found that the three critical factors contributing to Haiyan’s severe damage and high intensity, i.e., high sea level rise, warm water accumulation, and fast traveling speed, were all likely to be



(c)	Ivan (1997)	Joan (1997)	Megi (2010)	Haiyan (2013)
Peak intensity (kts)	160	160	160	170
Background state	El Niño	El Niño	La Niña	La Niña-like decadal condition
Genesis position	177°E 7°N	178.6°E 3.8°N	145°E 12.7°N	164.2°E 5.6°N
Distance from genesis to peak [km]	5446	3452	2425	4202
Avg. flux (genesis to Peak) [Wm ⁻²]	436	556	956	1025
Distance-integrated Flux [Wm ⁻² × km]	2,373,964	1,918,134	2,318,047	4,307,407

Figure 3. (a) The tracks (from genesis to peak) of Joan and Ivan (1997) overlaid on the long-term TC track composite during El Niño years (after Wang and Chan [2002]). (b) As in Figure 3a but for the tracks of Megi (2010) and Haiyan (2013) overlaid on the long-term TC track composite during La Niña years (after Wang and Chan [2002]). (c) Sub-table compares the background climate state, genesis position, distance over ocean, averaged flux, and distance-integrated flux for these four very intense supertypoons.

further analyses and compared Haiyan (2013), Megi (2010), with the two most intense TCs (Ivan and Joan, also peaked at 160 kts) found during the 1997 El Niño (Figure 3).

We first compare Megi with Ivan and Joan because they reached the same peak. As Megi formed during a La Niña year, its genesis position was much closer to land. As in Figure 3b, Megi had a much shorter intensification track (from genesis to peak, 2425 km), as compared to Ivan and Joan (5446 and 3452 km, Figures 3a and 3c). This observation in itself already shows that it is not always necessary to take a long track to reach the high intensity of 160 kts. Megi was able to reach the same peak in much shorter distance.

From the flux analyses (Figure 3c_sub-Table), it can be seen that there was much higher averaged flux supply for Megi, as compared to Ivan and Joan (956 W m⁻² vs. 436 and 556 W m⁻²). As in Figure S9a,

associated with the western Pacific manifestation of the La Niña-like decadal phenomenon. Therefore, Haiyan and the hiatus can coexist because they vaguely resemble the two sides of the same coin (the coin being the La Niña-like phenomenon). Our results also alert us the complexity in nature. Though we think that this phenomenon is to cool the planet via offsetting the global warming [Kosaka and Xie, 2013], it actually has another side of manifestation, the ability to fuel a record-breaking TC over the Asia Pacific [Peduzzi et al., 2012] region.

There is another interesting aspect worth noting, the comparison with the El Niño condition. Traditionally it is understood that it is El Niño, not La Niña, which favors these very intense TCs [Chan, 1985; Wang and Chan, 2002; Camargo and Sobel, 2005; Li and Zhou, 2012]. During El Niño, there is a south-eastward shift of TC forming positions (typically around 160°E–180°E, Figure 3a). Therefore TCs can travel longer distance and spend more time over ocean for intensification [Chan, 1985; Wang and Chan, 2002; Camargo and Sobel, 2005; Li and Zhou, 2012]. In La Niña years, TCs are usually formed much toward west (near land), typically at the west of 145°E [Wang and Chan, 2002; Camargo and Sobel, 2005]. There is thus less time and distance over ocean for intensification (Figure 3b).

However, both Haiyan (peak intensity 170 kts) and another very intense supertypoon, Megi in 2010 (peak intensity 160 kts), did not occur during El Niño. In fact, Megi (2010) occurred during a very strong La Niña year. How do we reconcile these? We conducted

Acknowledgments

This work is supported by the Ministry of Science and Technology (MOST), Taiwan. Thanks to Hsiao-Ching Huang, Ming Fang, Yi-Hsuan Hsieh for help in data processing and figure editing. Thanks also to the AVISO team, NOAA, ECMWF, JTWC, and the Central Weather Bureau (CWB, Dr. Ching-Tsi Feng and Mr. Yen-chi Shen) Taiwan, for providing essential data sets. Thanks to Wen Zhou and Richard Li (City University of Hong Kong) for helpful comments. Thanks a lot to the reviewers for their very constructive comments. We also thank the Editors and the production team for handling this paper. Finally, this work is a tribute to Bob Simpson, who proposed the Saffir-Simpson TC scale a few decades ago. The first author is greatly inspired by Simpson's talk during the American Meteorological Society's Hurricane conference in 2012. Though he was already 100 years old, his zeal and passion for science touched so many of us in the audience. Our very best wishes and sincere thanks to Bob Simpson.

The information of data used for this paper is listed below:

1. The historical western North Pacific typhoon best track data is available at the US Joint Typhoon Warning Center (JTWC). Data set: Best Track archive. URL: http://www.usno.navy.mil/NOOC/nmfc-ph/RSS/jtwc/best_tracks/
2. Haiyan's track and intensity data were the real time data by JTWC.
3. The ocean climatological temperature data were from NOAA's National Oceanographic Data Center (NODC). Data set: WOA01. URL: http://www.nodc.noaa.gov/OC5/WOA01/qd_ts01.html
4. The ocean in situ depth-temperature profiles were from NOAA's Global Temperature and Salinity Profile Program (GTSPP). Data Set: Best copy. URL: http://www.nodc.noaa.gov/GTSPP/access_data/gtspp-bc.html
5. The atmospheric wind data were from the European Centre for Medium Range Weather Forecasting (ECMWF). Data set: ERA Interim. URL: http://apps.ecmwf.int/datasets/data/interim_full_daily/
6. The SSHA data were from the AVISO team. Data sets: NRT-MSLA and DT MSLA "two sat merged". URL: <http://www.aviso.altimetry.fr/index.php?id=1272>
7. The long-term SST data were from NOAA. Data set: Weekly OISST. URL: ftp://ftp.emc.ncep.noaa.gov/cmb/sst/oisst_v2/
8. The atmospheric surface temperature and humidity data were from NOAA/NCEP. Data set: NCEP/NCAR Reanalysis 1. URL: <http://www.esrl.noaa.gov/psd/data/gridded/data.ncep.reanalysis.surface.html>

The Editor thanks Pao-Shin Chu and an anonymous reviewer for their assistance in evaluating this paper.

because Megi intensified over much warmer subsurface water during La Niña, the cooling effect was weaker (Figure S9b), and the flux supply was higher (Figure S9c). Therefore, Megi's shorter distance was compensated by the higher flux supply. As a result, the final distance-integrated fluxes for the three supertyphoons were similar (Figure 3c_sub-Table).

These results suggest that with sufficiently high flux supply, it does not appear to be necessary to travel such long distance to reach the same intensity. Certainly, it is no harm and is even better if a TC can also travel the long distance. This is the situation found in Haiyan; one sees that its flux supply was even higher than Megi (Figure 3c_sub-Table and S9). Furthermore, its genesis position was much eastward, $\sim 164^\circ\text{E}$. It could thus take the benefits from both high flux supply and long distance over ocean. The end result is the even higher peak intensity and distance-integrated flux for Haiyan, as compared with the other three cases (Figure 3).

Therefore not only El Niño, La Niña could also support intensification for these very intense supertyphoons. Certainly, the most optimal intensification situation (though the most dangerous to people) would be the situation encountered by Haiyan, i.e., occurring during a La Niña-like condition over the western North Pacific to take advantage for the warm ocean (for both SST and the subsurface ocean. Stronger warming is found in the subsurface (Figure 2a) than SST) (Figure S6)).

Also, because this ongoing La Niña-like decadal phenomenon is most likely of natural, multi-decadal origin [Cazenave and Remy, 2011; Qiu and Chen, 2012; Kosaka and Xie, 2013; Wang et al., 2013; Pun et al., 2013; England et al., 2014], there is less direct evidence to support the link between Haiyan and the anthropogenic global warming.

Finally, as in the introduction, Haiyan's intensity of 170 kts was much higher than most of the existing category 5 supertyphoons (peaked mostly at ~ 140 – 145 kts) [Lin et al., 2008; Knapp et al., 2010; Lander et al., 2014]. In the Saffir-Simpson scale, the gap between the threshold (minimum) values for each consecutive category is about 13–22 kts and the category 5 threshold is 135 kts (Table 1a). Therefore, even if adding another 20 kts above category 5 threshold to form a new category "6" with a threshold value of 155 kts, Haiyan's 170 kts intensity is still 15 kts well above the "category 6" threshold (Table 1a). Not only wind speed, it is also worthwhile to consider the wind speed cube (Table 1b). As suggested by Southern [1979] and Emanuel [2005], the actual monetary loss in wind storms rises roughly with wind speed cube. Wind speed cube is also an important factor in estimating TC's destructive potential (characterized by the Power Dissipation Index, PDI [Emanuel, 2005]). Haiyan's landfall wind speed cube (cube of 170 kts) would be 180% as compared to the landfall wind speed cube of a regular category 5 TC of 140 kts (Table 1b). This is a large percentage increase in wind speed cube and the potential in damage and loss. It can be risky if the public equate Haiyan with a regular category 5 TC. However, since currently there is no category "6," Haiyan is indeed still categorized as category 5 at landfall. Though currently there is no category "6" in the Saffir-Simpson scale and to form a new category requires consideration from many different perspectives/concerns, it may be worthwhile to re-consider such possibility, as more accurate information can be communicated. Finally, Saffir-Simpson scale is based on TC intensity and wind speed. Certainly, not only TC wind but also other TC-related factors (such as rainfall, surge, ...) are also critical. Eventually, it will be very helpful if these different aspects of information can be well-synthesized and accurately communicated, especially over the Asia-Pacific region where the TC-related impact is the highest in the world.

References

- Bender, M. A., and I. Ginis (2000), Real case simulation of hurricane-ocean interaction using a high-resolution coupled model: Effects on hurricane intensity, *Mon. Weather Rev.*, **128**, 917–946.
- Camargo, S. J., and A. H. Sobel (2005), Western North Pacific tropical cyclone intensity and ENSO, *J. Clim.*, **18**, 2996–3006.
- Cazenave, A., and F. Remy (2011), Sea level and climate: Measurements and causes of changes, *Wires Clim. Change*, **2**, 647–662.
- Chan, J. C. L. (1985), Tropical cyclone activity in the northwest Pacific in relation to the El Niño/Southern Oscillation phenomenon, *Mon. Weather Rev.*, **113**, 599–606.
- Cione, J. J., and E. W. Uhlhorn (2003), Sea surface temperature variability in hurricanes: Implications with respect to intensity change, *Mon. Weather Rev.*, **138**(8), 1783–1796, doi:10.1175/2562.1.
- Cione, J. J., E. A. Kalina, J. A. Zhang, and E. W. Uhlhorn (2013), Observations of air-sea interaction and intensity change in hurricanes, *Mon. Weather Rev.*, **141**(7), 2368–2382, doi:10.1175/MWR-D-12-00070.1.
- Emanuel, K. A. (1988), The maximum intensity of hurricanes, *J. Atmos. Sci.*, **45**, 1143–1155.
- Emanuel, K. A. (1999), Thermodynamic control of hurricane intensity, *Nature*, **401**, 665–669.
- Emanuel, K. A. (2005), Increasing destructiveness of tropical cyclones over the past 30 years, *Nature*, **436**, 686–688.
- Emanuel, K. A., C. DesAutels, C. Holloway, and R. Korty (2004), Environmental control of tropical cyclone intensity, *J. Atmos. Sci.*, **61**, 843–858.

- England, M. H., S. McGregor, P. Spence, G. A. Meehl, A. Timmermann, W. Cai, A. S. Gupta, M. J. McPhaden, A. Purich, and A. Santoso (2014), Recent intensification of wind-driven circulation in the Pacific and the ongoing warming hiatus, *Nature Clim. Change*, *4*, 222–227.
- Forbes, C., R. A. Luettich Jr., C. Mattocks, and J. J. Westerink (2010), A retrospective evaluation of the storm surge produced by Hurricane Gustav (2008): Forecast and hindcast results, *Weather Forecasting*, *25*, 1577–1602.
- Frank, W. M., and E. A. Ritchie (2001), Effects of vertical wind shear on the intensity and structure of numerically simulated hurricanes, *Mon. Weather Rev.*, *129*, 2249–2269.
- Goni, G. J., et al. (2009), Applications of satellite-derived ocean measurements to tropical cyclone intensity forecasting, *Oceanography*, *22*, 190–197.
- Gray, W. M. (1979), Hurricanes: Their formation, structure and likely role in the tropical circulation, in *Meteorology Over the Tropical Oceans*, pp. 155–218, James Glaisher House, Grenville Place, Bracknell, Berkshire, RG12 1BX.
- Knapp, K. R., M. C. Kruk, D. H. Levinson, H. J. Diamond, and C. J. Neumann (2010), The international best track archive for climate stewardship (IBTrACS): Unifying tropical cyclone best track data, *Bull. Am. Meteorol. Soc.*, *91*, 363–376.
- Kosaka, Y. (2014), Increasing wind sinks heat, *Nature Clim. Change*, *4*, 172–173.
- Kosaka, Y., and S. P. Xie (2013), Recent global warming hiatus tied to equatorial Pacific surface cooling, *Nature*, *501*, 403–407.
- Lander, M., C. Guard, and S. J. Camargo (2014), Tropical cyclones, super-typhoon Haiyan, in *State of the Climate in 2013*, *Bull. Am. Meteorol. Soc.*, *95*, S112–S114.
- Leipper, D., and D. Volgenau (1972), Hurricane heat potential of the Gulf of Mexico, *J. Phys. Oceanogr.*, *2*, 218–224.
- Li, R. C. Y., and W. Zhou (2012), Changes in western Pacific tropical cyclones associated with the El Niño–Southern Oscillation cycle, *J. Clim.*, *25*, 5864–5878.
- Lin, I. I., C. C. Wu, K. Emanuel, I. H. Lee, C. R. Wu, and I. F. Pun (2005), The interaction of Supertyphoon Maemi (2003) with a warm ocean eddy, *Mon. Weather Rev.*, *133*(9), 2635–2649.
- Lin, I. I., C. C. Wu, I. F. Pun, and D. S. Ko (2008), Upper-ocean thermal structure and the western North Pacific category 5 typhoons. Part I: Ocean features and the category 5 typhoons' intensification, *Mon. Weather Rev.*, *136*, 3288–3306.
- Lin, I. I., I. F. Pun, and C. C. Wu (2009), Upper ocean thermal structure and the western North Pacific category-5 typhoons. Part II: Dependence on translation speed, *Mon. Weather Rev.*, *137*, 3744–3757.
- Lin, I. I., P. Black, J. F. Price, C. Y. Yang, S. S. Chen, C. C. Lien, P. Harr, N. H. Chi, C. C. Wu, and E. A. D'Asaro (2013a), An ocean coupling potential intensity index for tropical cyclones, *Geophys. Res. Lett.*, *40*, 1878–1882, doi:10.1002/grl.50091.
- Lin, I. I., G. J. Goni, J. Knaff, C. Forbes, and M. M. Ali (2013b), Ocean heat content for tropical cyclone intensity forecasting and its impact on storm surge, *Nat. Hazards*, *66*(3), 1481–1500.
- Mori, N., M. Kato, S. Kim, H. Mase, Y. Shibutani, T. Takemi, K. Tsuboki, and T. Yasuda (2014), Local amplification of storm surge by Super Typhoon Haiyan in Leyte Gulf, *Geophys. Res. Lett.*, *41*, 5106–5113, doi:10.1002/2014GL060689.
- Peduzzi, P., B. Chatenoux, H. Dao, A. De Bono, C. Herold, J. Kossin, F. Mouton, and O. Nordbeck (2012), Global trends in tropical cyclone risk, *Nature Clim. Change*, *2*, 289–294.
- Price, J. F. (1981), Upper ocean response to a hurricane, *J. Phys. Oceanogr.*, *11*, 153–175.
- Price, J. F. (2009), Metrics of hurricane-ocean interaction: Vertically-integrated or vertically-averaged ocean temperature?, *Ocean Sci.*, *5*, 351–368.
- Price, J. F., T. B. Sanford, and G. Z. Forristall (1994), Forced stage response to a moving hurricane, *J. Phys. Oceanogr.*, *24*, 233–260.
- Pun, I. F., I. I. Lin, C. R. Wu, D. S. Ko, and W. T. Liu (2007), Validation and application of altimetry-derived upper ocean thermal structure in the western north pacific ocean for typhoon intensity forecast, *IEEE Trans. Geosci. Remote Sens.*, *45*, 1616–1630.
- Pun, I. F., I. I. Lin, and M. H. Lo (2013), Recent increase in high tropical cyclone heat potential area in the Western North Pacific Ocean, *Geophys. Res. Lett.*, *40*, 4680–4684, doi:10.1002/grl.50548.
- Pun, I. F., I. I. Lin, and D. S. Ko (2014), New generation of satellite-derived ocean thermal structure for the Western North Pacific typhoon intensity forecasting, *Prog. Oceanogr.*, *121*, 109–124, doi:10.1016/j.pocan.2013.10.004.
- Qiu, B., and S. Chen (2012), Multi-decadal sea level and gyre circulation variability in the northwestern tropical Pacific Ocean, *J. Phys. Oceanogr.*, *42*, 193–206.
- Seo, H., and S. P. Xie (2013), Impact of ocean warm layer thickness on the intensity of hurricane Katrina in a regional coupled model, *Meteorol. Atmos. Phys.*, *122*, 19–32.
- Shay, L. K., G. J. Goni, and P. G. Black (2000), Role of a warm ocean feature on Hurricane Opal, *Mon. Weather Rev.*, *128*, 1366–1383.
- Southern, R. L. (1979), The global socio-economic impact of tropical cyclones, *Aust. Meteorol. Mag.*, *27*, 175–195.
- Wang, B., and J. C. L. Chan (2002), How ENSO regulates tropical storm activity over the western North Pacific, *J. Clim.*, *15*, 1643–1658.
- Wang, B., J. Liu, H.-J. Kim, P. J. Webster, S.-Y. Yim, and B. Xiang (2013), Northern Hemisphere summer monsoon intensified by mega-El Niño/Southern Oscillation and Atlantic multidecadal oscillation, *Proc. Natl. Acad. Sci. U.S.A.*, *110*, 4347–4352.
- Yablonski, R. M., and I. Ginis (2008), Improving the ocean initialization of coupled hurricane-ocean models using feature-based data assimilation, *Mon. Weather Rev.*, *136*, 2592–2607.

Supporting Online Material for:

‘Category-6’ Supertyphoon Haiyan in

Global Warming Hiatus: Contribution from Subsurface Ocean Warming

(by Lin et al.)

S1. Data and Method:

1. Study area: 122-180°E, 4-19°N, i.e., the southern part of the western North Pacific typhoon Main Development Region, see box in Figs. 1bc.

2. Data sets:

a. Atmospheric environmental wind condition: the operational, 12 hourly, 0.5 degree grid data from the European Centre for Medium-Range Weather Forecasts (ECMWF) was used for Haiyan. For long-term climatological analysis, 20 years’ (1993-2012) of ECMWF Interim Reanalysis data set at daily, 1.5 degree grid was used.

b. TC track and intensity data: Haiyan’s track and intensity was from the US Joint Typhoon Warning Centre (JTWC)’s operational warning track. For historical TC data from 1970 to 2011, JTWC’s best track data was used.

c. Ocean depth-temperature profiles: ocean thermal profiles from the Argo in situ floats [Gould et al., 2004] were used to characterize ocean’s pre-existing condition for Haiyan. Profiles were searched along Haiyan’s track within 5 days prior to Haiyan’s passing. For reference and comparison, US NOAA (National Oceanic and Atmospheric Administration)’s World Ocean Atlas 2001 (WOA01) [Stephens et al., 2002] data set was used for the climatological ocean condition. For Megi (2010), Joan and Ivan (1997), the profiles were searched from the NOAA Global Temperature-Salinity Profile Program data base.

d. Ocean surface atmospheric temperature (T_a) and humidity (q_a) data: operational, 6 hourly, 2.5 degree grid data from the US NCEP (National Center for Environmental Prediction) was used.

e. Long-term sea surface temperature (SST) data: NOAA's Optimum Interpolation SST data base [Reynolds et al., 2002] between 1993 and 2013 was used.

f. Long-term ocean subsurface thermal information: two parameters, i.e., the depth of the 26 degree C isotherm (D26) and TCHP were used. Both parameters are the well-known parameters to characterize the upper ocean subsurface thermal condition for TC intensification [Shay et al., 2000; Lin et al., 2008; Goni et al., 2009]. D26 is a common measure of the subsurface warm layer thickness. TCHP is defined as the integrated heat content from SST .wrt. D26 and is a measure of the subsurface heat reservoir [Shay et al., 2000; Goni et al., 2009]. Using SST and satellite altimetry sea surface height anomaly (SSHA) observations, we use the algorithm developed by Shay et al. [2000] to estimate D26 and TCHP. This approach has been validated for the western North Pacific Ocean using several thousand in situ Argo float observations [Pun et al., 2007]. Also, as the altimetry SSHA measurements include the contributions from both the thermal and mass components [Cazenave and Remy, 2011], Gravity Recovery and Climate Experiment (GRACE) satellite data are used to quantify the mass contribution [Chambers, 2006]. After removal of the mass contribution in SSHA, the remaining SSHA (i.e., the thermal SSHA component) is then used to calculate D26 and TCHP (details see Pun et al., 2013).

3. Cooling effect estimation: cooling effects were simulated under 4 scenarios (Fig. S4). Scenario 1: the observed scenario (with pre-existing warm water accumulation and fast TC travelling speed of 8.9 m s^{-1}). Scenario 2: normal ocean but with fast TC travelling speed (in green). Scenario 3: with warm water accumulation but normal travelling speed 5 m s^{-1} (in blue). Scenario 4: normal ocean and normal TC travelling speed (in brown). The input for Scenarios 1 and 3 used the in situ Argo profiles (i.e. red profiles in Fig. 2b). For Scenarios 2 and 4, the reference climatological profiles (i.e. black profiles in Fig. 2b) were used. The model is the 3DPWP model [Price et al., 1986, 1994]. This model solves for the wind-driven, baroclinic ocean response, including a treatment of turbulent vertical mixing in the upper ocean. The horizontal resolution was 5 km and the vertical resolution was 5 m. The 2D wind field input was calculated based on the maximum intensity and radius of maximum wind information from JTWC's best track data.

4. Air-sea flux calculation: as in the main text, SHF and LHF are calculated separately from the bulk aerodynamic formula. The input of the during-intensification SST is the SST with consideration of the cooling effect (i.e. Fig. S4). T_a and q_a are from the NCEP data set. The exchange coefficients are from Black et al. [2007]. The wind speed was from JTWC. As in Fig. S5 and Table S1, the stronger the cooling effect, the smaller the air-sea temperature and humidity difference (Figs. S5ab), the smaller the sensible and latent heat fluxes correspond (Figs. S5cd).

5. Atmospheric vertical wind shear: vertical wind shear was calculated based on the azimuthal average of the 200 hPa minus 850 hPa wind difference in a 200-800 km annulus centred at TC. The 6 hourly reanalysis data from the ECMWF Interim data set was used.

S2. The fast traveling speed of Haiyan:

As in Fig. 1d, the prevailing environmental wind condition during Haiyan's intensification period (3-7 November 2013) was characterized by strong easterly wind of more than 10 ms^{-1} . As in Fig. S3, this easterly wind was about 4 ms^{-1} stronger than climatology. The strong, prevailing easterly wind pushed Haiyan to travel fast towards the Philippines (Fig. 1c). As also can be seen from 21 years' of observations, the steering flow (averaged from 850 to 500 hPa over the study domain) for Haiyan was the fastest (Fig. 2a). This steering flow of about 9 ms^{-1} easterly wind, was consistent with the observed 8.9 ms^{-1} traveling speed of Haiyan.

S3. Accumulation of warm water at the east of the Philippines:

As in Figs. 1ab and 2a, the La Niña like decadal phenomenon has much piled up warm water to the western North Pacific, especially over the study region at the east of the Philippines (see box in Fig. 1bc). This region is located at the southern part of the typhoon Main Development Region (MDR) (Pun et al. 2013). The TCHP result in Fig. 2a is after the mass correction (see Method). Fig. S7 depicts the result for D26 and TCHP, before and after removal of the mass contribution. Fig. S6 illustrates the 21 years' time series of SST over the same region.

S4. Atmospheric vertical wind shear condition for Haiyan:

Vertical wind shear is an important factor to TC intensification and the shear condition for Haiyan was examined. It was found that the shear condition for Haiyan was not as optimal. Shear was relatively large ($\sim 9 \text{ m s}^{-1}$) in the beginning of Haiyan's genesis, but decreased subsequently (1-3 Nov., Fig. S8). It increased rapidly again to about 10 ms^{-1} in the first half of the intensification period (3-5 Nov.) but decreased to about 5 ms^{-1} , as Haiyan continued to intensify to its peak. It appears that though there were unfavorable periods with relatively large shear, Haiyan was still able to intensify. In short, the shear condition for Haiyan was not particularly favourable, but Haiyan's intensification was not found to be hindered (Fig. S8).

S5. Cooling effect and air-sea enthalpy flux for the 4 super-typhoon cases (Ivan, Joan, Megi and Haiyan):

To compare the difference in the cooling effect and enthalpy flux supply for the 4 super-typhoons, further analyses were performed. As in Fig. 3, Ivan and Joan (both in October 1997) occurred during El Niño while Megi (October 2010) and Haiyan (November 2013) occurred during La Niña and La Niña-like conditions. The results are illustrated in Figs. 3 and S9. It can be seen in Fig. S9a that the ocean subsurface thermal condition was more favorable for the La Niña and the La Niña-like cases (i.e. Megi and Haiyan). As a result, the TC-induced cooling effect (Fig. S9b) was also weaker and there was higher enthalpy flux supply for Megi and Haiyan, as compared to Ivan and Joan.

Additional references:

- Black, P. G., E. A. D'Asaro, W. M. Drennan, J. R. French, P. P. Niller, T. B. Sanford, E. J. Terrill, E. J. Walsh, and J. A. Zhang (2007), Air-sea exchange in hurricanes, *Bull. Amer. Meteor. Soc.*, 88, 357-374.
- Chambers, D. P. (2006), Observing seasonal steric sea level variations with GRACE and satellite altimetry, *J Geophys Res*, 111.
- Gould, J. *et al.* (2004), Argo profiling floats bring new era of in situ ocean observations, *EOS (Trans. Am. Geophys. Union)* 85, 190-191.
- Price, J. F., R. A. Weller, and R. Pinkel (1986), Diurnal cycling: observations and models of the upper ocean response to diurnal heating, cooling, and wind mixing. *J. Geophys. Res.*, 91, 8411-8427.

- Pun, I. F., Lin, I. I., Wu, C. R., Ko, D. S. and Liu, W. T. (2007), Validation and application of altimetry-derived upper ocean thermal structure in the western North Pacific ocean for typhoon intensity forecast, *IEEE Trans. Geosci. Remote Sens.* 45, 1616-1630.
- Reynolds, R. W., Rayner, N. A., Smith, T. M., Stokes, D. C., and Wang, W. Q. (2002), An improved in situ and satellite SST analysis for climate. *J Climate*, 15, 1609-1625.
- Stephens, C., J. I. Antonov, T. P. Boyer, M. E. Conkright, R. A. Locarnini, T. D. O'Brien, and H. E. Garcia (2002), World ocean atlas 2001 volume 1: temperature, S. Levitus, Ed., NOAA Atlas NESDIS 49. U. S. Government Printing Office, Washington, D. C.

Supplementary table:

Scenario	SHF (W m⁻²)	LHF (W m⁻²)	Enthalpy (SHF+LHF) flux (W m⁻²)
1	169	1153	1322
2	137	1034	1171
3	118	990	1108
4	64	774	838
5	-46	965	920

Scenario 1 (i.e. the observed scenario for Haiyan) is thus of 484 W m⁻² higher supply as compared to scenario 4. Therefore the supply for scenario 1 was 158% (1322/838) of the normal supply.

Table S1: Corresponding to Figs. 2c and S5, the averaged SHF, LHF, and enthalpy (SHF+LHF) heat fluxes for the 5 scenarios.

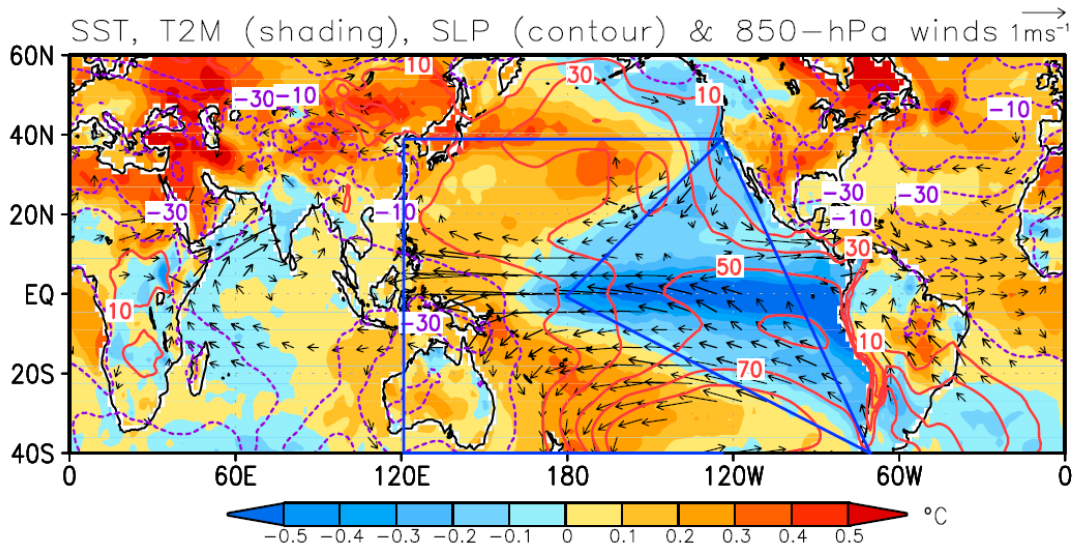


Fig. S1: Characteristics of the ongoing La Niña-like decadal phenomenon: cooling over the eastern tropical Pacific, strong easterly wind, and the associated piling up of warm water to the western Pacific. Four climate anomaly fields are shown. They are the regressed anomaly field associated with the Northern Hemisphere Summer Monsoon circulation index between 1979 and 2010. The colour shading is for SST anomaly (over ocean) and 2-m air temperature anomaly (over land). The wind vector is the 850 hPa vector wind anomaly. The contour is the sea level pressure anomaly (after Wang et al. [2013]).

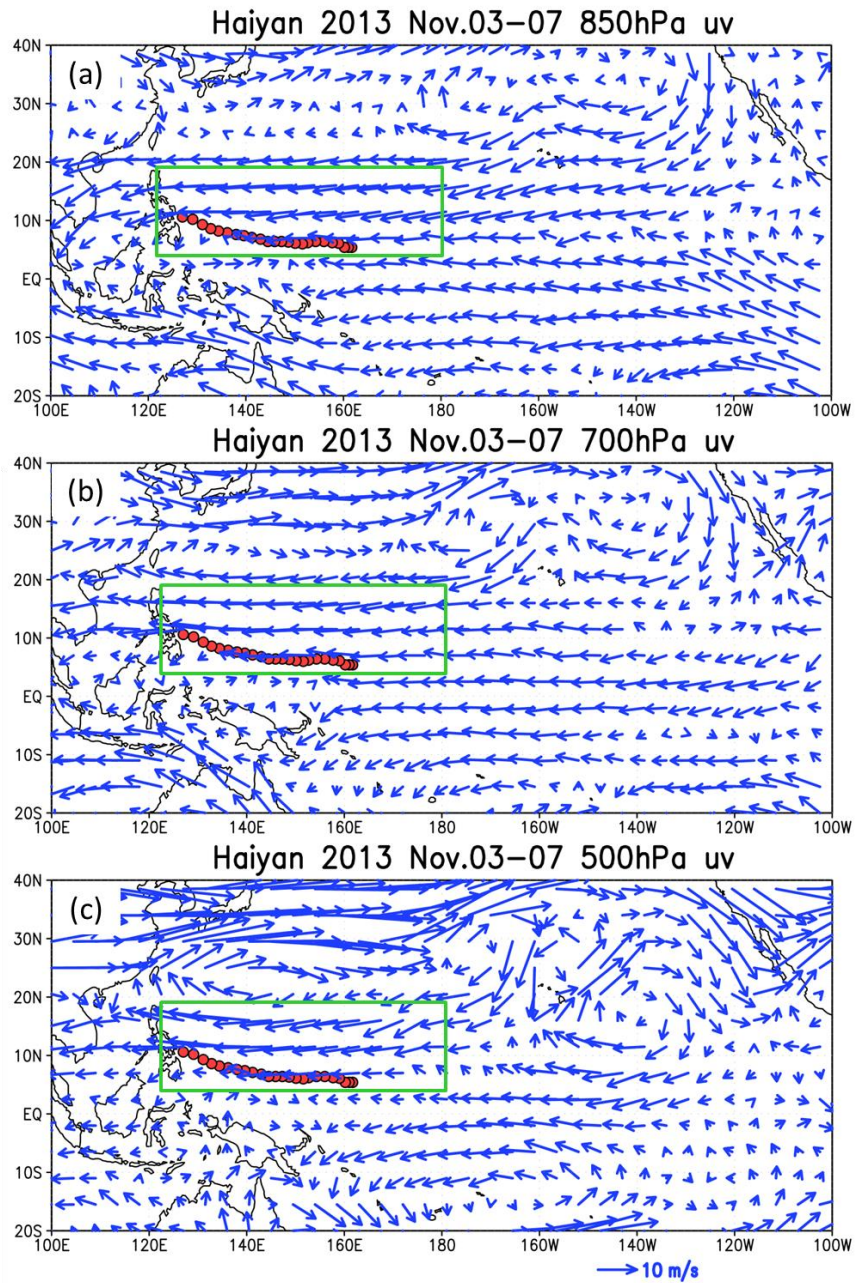


Fig. S2: Prevailing environmental wind condition during Haiyan’s intensification period (3-7 November 2013), at 850, 700, and 500 hPa, respectively. The track and the intensification location (see box) of Haiyan are also depicted. Data source: ECMWF operational atmospheric data.

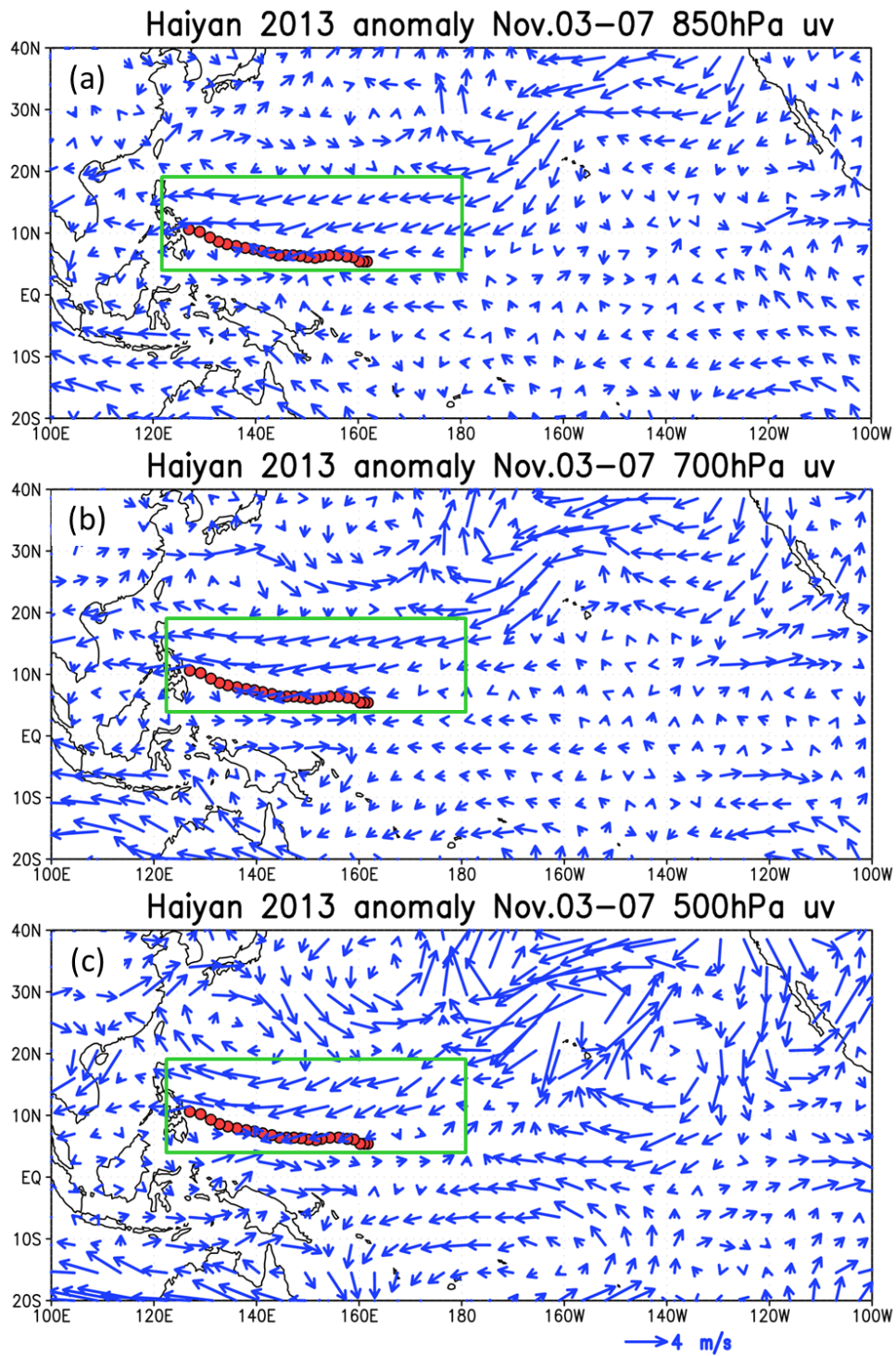


Fig. S3: As in Fig. S2, but for the anomaly .wrt. climatology. Data source: ECMWF interim and operational data sets.

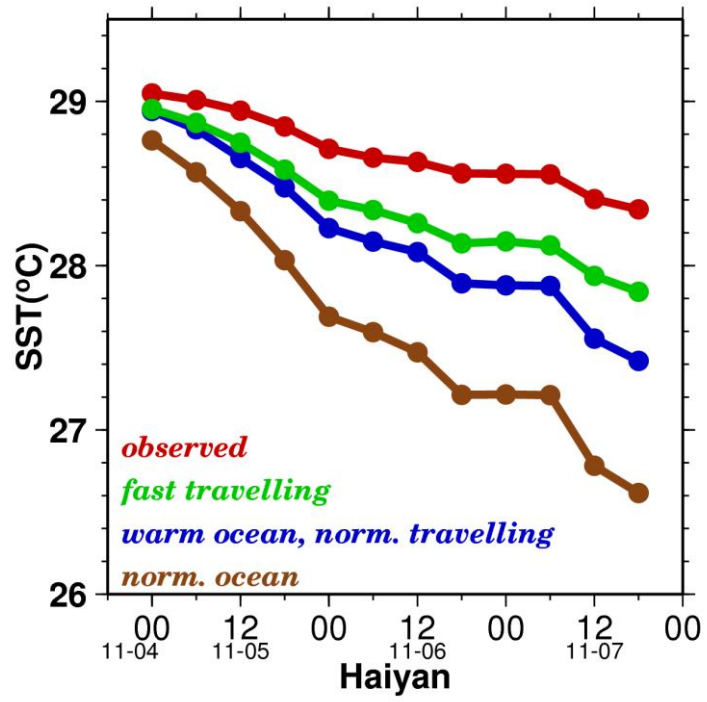


Fig. S4: Simulation of cooling effect for the 4 scenarios, as simulated by the 3DPWP model.

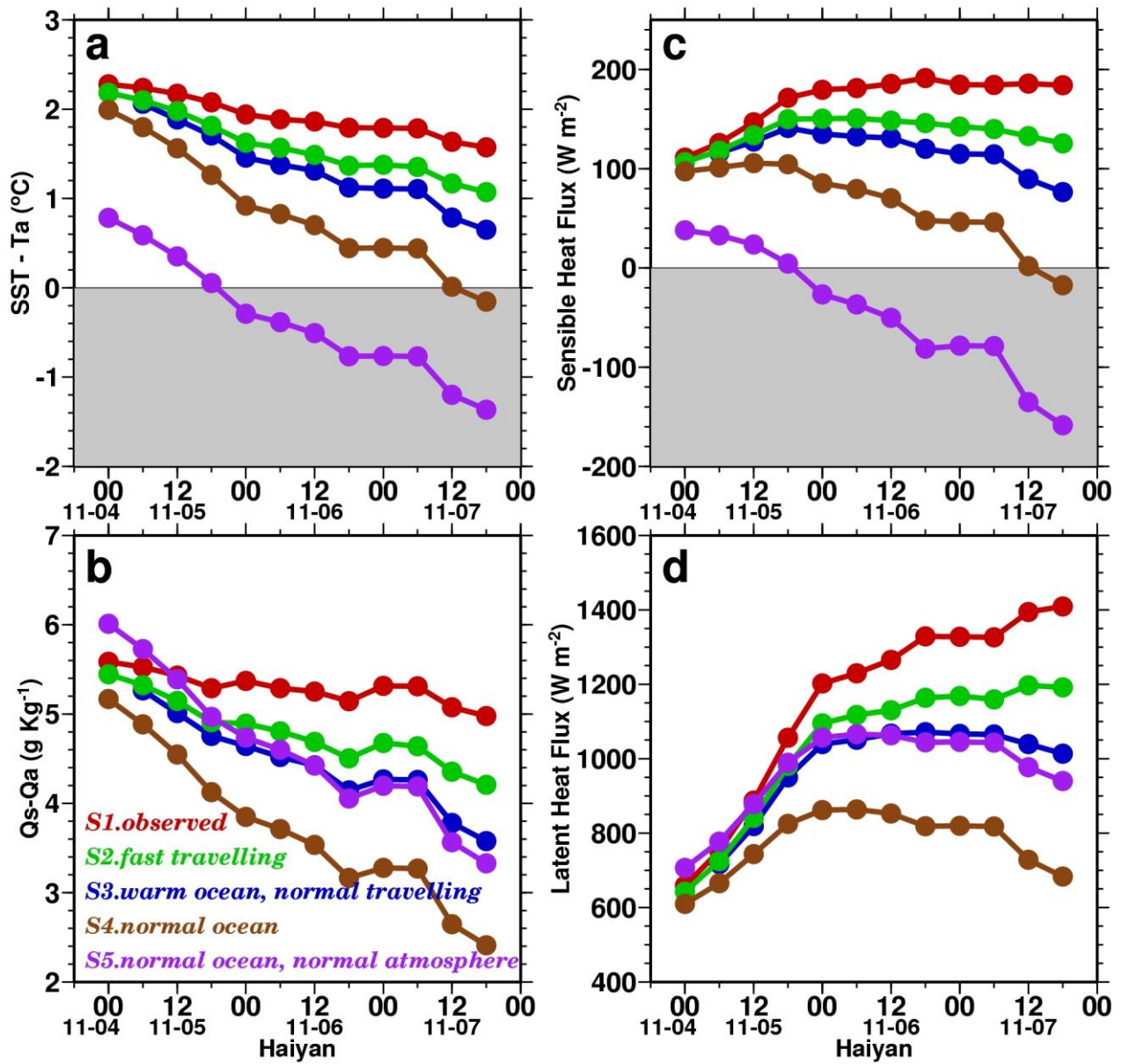


Fig. S5: As in Fig. 2c, but for the corresponding atmospheric and ocean temperature and humidity differences (a, b). The corresponding SHF and LHF are in (c, d).

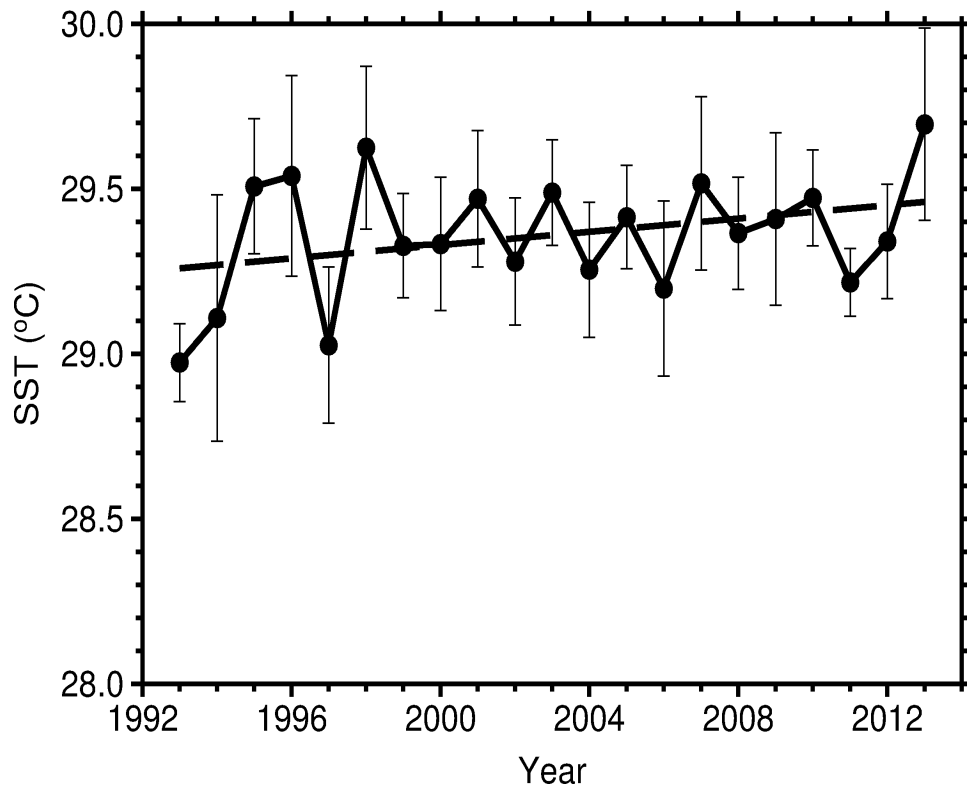


Fig. S6: As in Fig. 2a, but for the SST between 1993 and 2013.

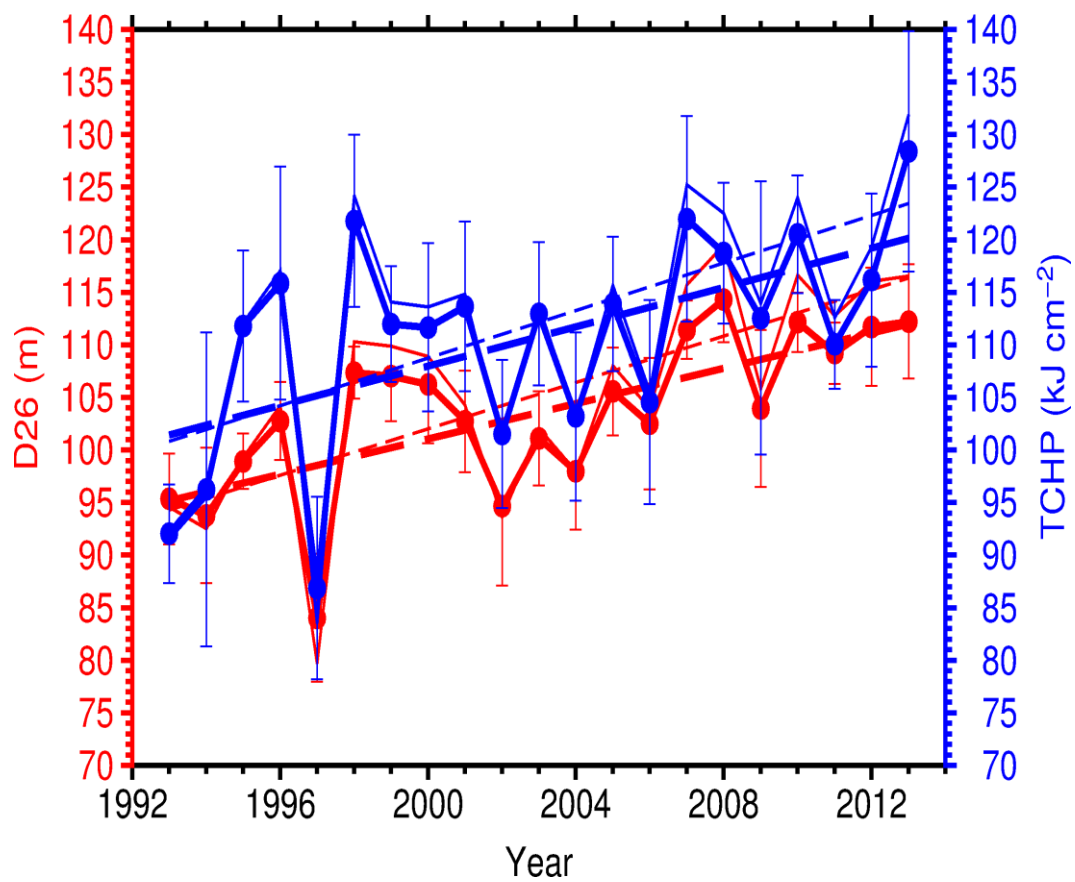


Fig. S7: As in Fig. 2a, but for D26 and TCHP, comparison before (thin) and after (thick) the mass correction (see Method).

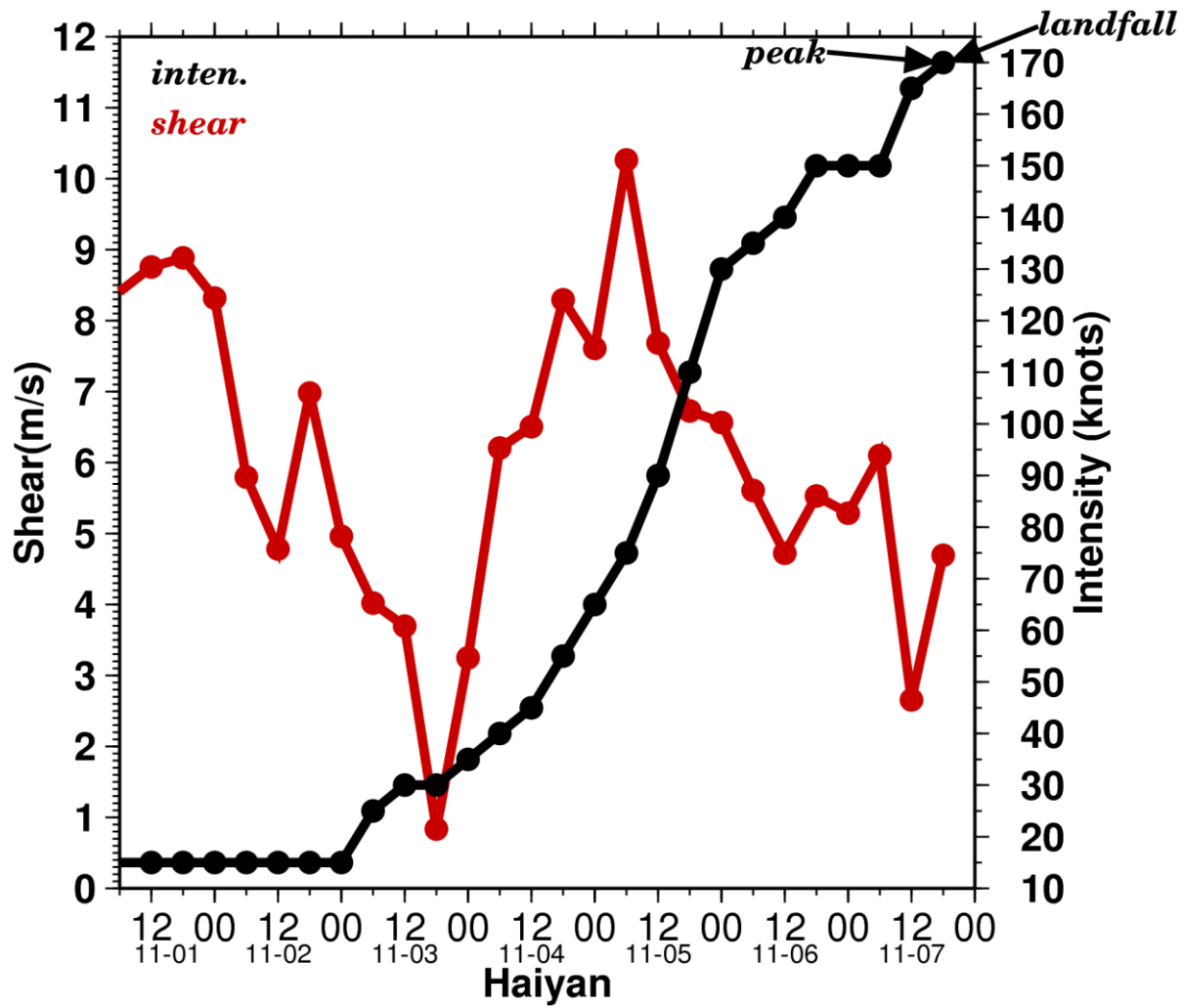


Fig. S8: Evolution of the atmospheric vertical wind shear (red) .wrt. Haiyan’s genesis and intensification (black) from 1-7 Nov. 2013.

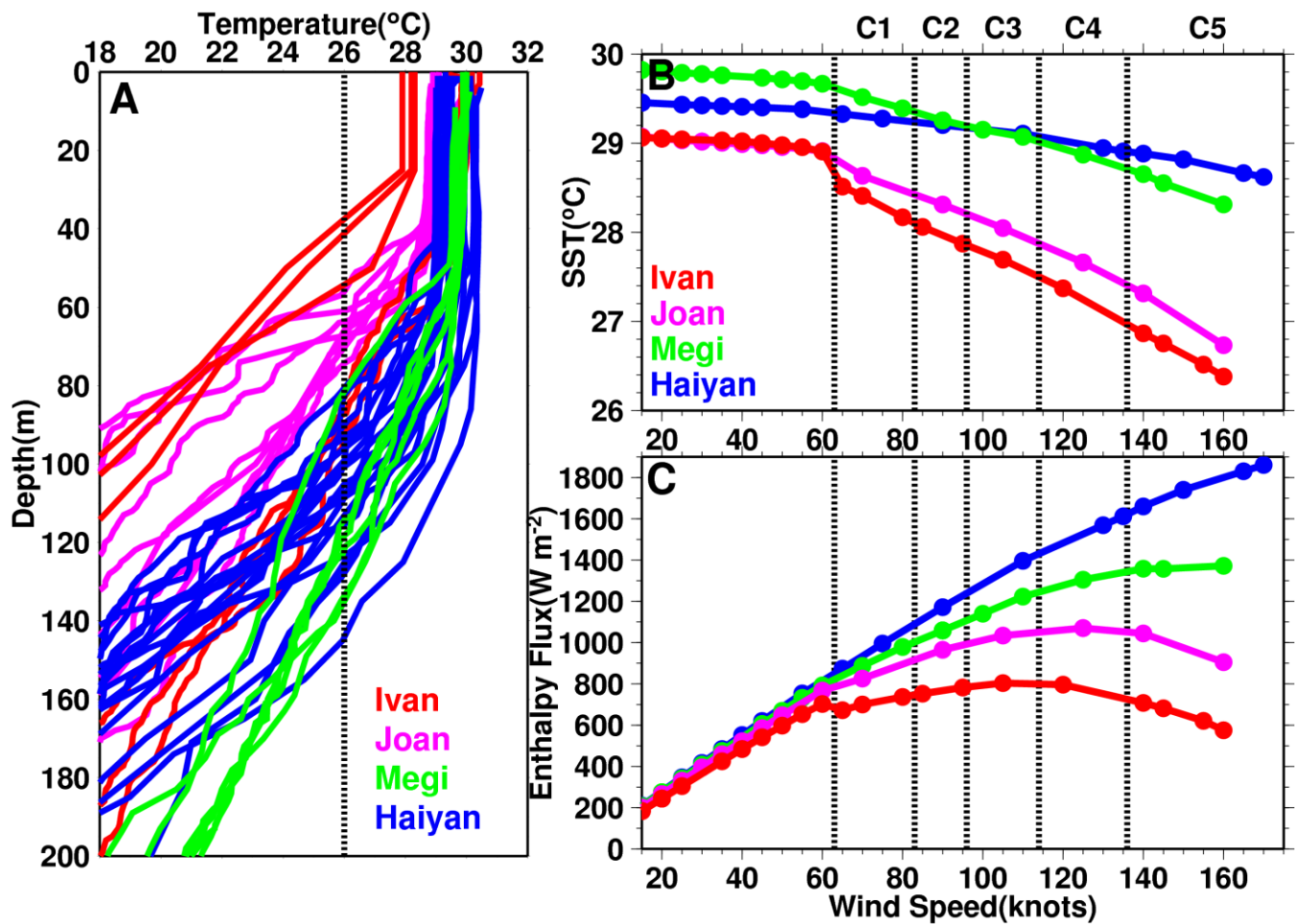


Fig. S9: (a) Pre-typhoon initial ocean depth-temperature profiles for the 4 super-typhoon cases. The profiles (locations see Figs. 3ab) were searched within 300 km from the TC tracks. The searching time window was within 1 week before the genesis date for each case. (b) During-intensification SST cooling simulated by the 3DPWP model for the 4 cases. (c) As in (b), but for the corresponding air-sea enthalpy flux.